Comparison of Raman and IR spectroscopy for quantitative analysis of gasoline/ethanol blends

Corsetti, Stella; McGloin, David; Kiefer, Johannes

Published in:
Fuel

DOI:
10.1016/j.fuel.2015.11.018

Publication date:
2016

Document Version
Peer reviewed version

Comparison of Raman and IR spectroscopy for quantitative analysis of gasoline/ethanol blends

Stella Corsetti [a,b], David McGloin [b], Johannes Kiefer [a,c,d,*]

[a] School of Engineering, University of Aberdeen, Fraser Noble Building, Aberdeen AB24 3UE, Scotland, United Kingdom

[b] SUPA, School of Science and Engineering, University of Dundee, Nethergate, Dundee DD1 4HN, Scotland, United Kingdom

[c] Technische Thermodynamik, Universität Bremen, Badgasteiner Str. 1, 28359 Bremen, Germany

[d] Erlangen Graduate School in Advanced Optical Technologies (SAOT), Universität Erlangen-Nürnberg, Erlangen, Germany

*Corresponding author: jkiefer@uni-bremen.de

Abstract

Ethanol is commonly admixed to petrochemical gasoline, and its amount in the fuel blend can influence the performance of an engine. The ethanol content in a commercial fuel can vary. To ensure reliable engine operation, control strategies based on a measurement of the composition need to be developed. Two possible methods to determine the ethanol content in ethanol/gasoline blends are Raman and IR spectroscopy. We compare both techniques for quantitative measurements in systematically varied blends of ethanol and a gasoline surrogate. For each method, two different approaches for data evaluation are tested and compared: Firstly, the calibration of the intensity ratio of characteristic peaks as function of composition; secondly, a principal component regression (PCR). Both methods are found to have comparable uncertainty. For the evaluation of the Raman spectra, the PCR method yielded better accuracy than the intensity ratio approach. In addition, a detailed investigation of the influence of noise in the signal is presented. When the full IR spectra were evaluated by PCR, even high noise levels did not reduce the measurement accuracy significantly.

1 Introduction

The recent interest in bioethanol as fuel is due to strategies to reduce the impact of greenhouse gas emissions from the transport sector and to reduce dependency on fossil fuels. Bioethanol is mainly produced by fermentation of agriculture feedstocks (e.g. sugar cane, sugar beet and corn) but the future trend is the production of ethanol from non-food biomass [1]. The world's largest producers of bioethanol are the United States and the largest exporter is Brazil [2]. The main bioethanol producing European countries are Germany, France, Italy, and Spain [3].

Bioethanol is probably the most widely used alternative automotive fuel in the world. It possesses interesting properties for spark ignition engine operation, for example it reduces the net CO_2 emissions and has a high antiknock power [4]. However, its high latent heat of vaporization alters the volatility of the mixture and hence its evaporation behavior [5], especially if the fuel is used in geographical areas that are particularly cold. For use as an automotive fuel, it is often blended with gasoline in percentages from 5% to 85% by volume. Mixtures with an ethanol content up to 7.5% by volume can be used without making any changes to the engine (complete interchangeability). If the purity of anhydrous ethanol is high enough to avoid the presence of water causing the phase separation of ethanol and gasoline, mixtures containing up to 16.5% can be used in spark ignition (SI) engines without any modifications [6].

The amount of ethanol in a fuel blend is a crucial parameter, as it influences the engine performance directly [7, 8]. Therefore, its accurate and fast determination is an important task. Gas and liquid chromatography are commonly used for this purpose [9-11]. However, chromatographic methods

normally share the disadvantage that they are relatively slow and thus do not allow real-time monitoring of the fuel quality. This disadvantage can be overcome by spectroscopic techniques such as Raman and infrared (IR) spectroscopy. Their use for fuel characterization has recently been reviewed [12]. Due to different underlying physical phenomena, Raman and IR spectroscopy represent complementary techniques commonly employed to analyze molecular structure. For compositional analysis of hydrocarbon fuels, either method is normally sufficient. However, the best method for a given measurement task has to be chosen carefully.

Vibrational spectroscopic methods were used to analyze blends of ethanol and gasoline (surrogates) qualitatively and quantitatively in a number of studies. Van Ness et al.[13] applied IR spectroscopy to binary solutions of ethanol with heptane or toluene using IR spectroscopy. They derived information about the thermodynamics and the molecular structure of the mixtures by putting the spectra into context with heats of mixing. Infrared and excess infrared spectroscopy was used by Corsetti et al.[14] to examine molecular interactions and microscopic mixing effects in blends of ethanol and a gasoline surrogate comprising heptane and iso-octane. Measuring the ethanol content in blends was briefly touched in [14] as well using approaches based on the Beer-Lambert law. Such quantitative measurements, however, are more common when mixtures containing real gasoline are investigated spectroscopically. For this purpose, Raman[15], IR[16-18], and NIR[19] spectra were exploited. All these methods have been found suitable in these studies. However, a systematic comparison of the techniques has not been performed to date, to the best of the authors' knowledge.

This work compares Raman and IR spectroscopy for the determination of the ethanol content in fuel blends. Samples with systematically varied ratios of ethanol and a gasoline surrogate (i.e. a mixture of n-heptane and iso-octane) have been prepared. A set of spectra from each sample has been recorded with both methods. In a previous article,[14] the IR and excess IR spectra were analyzed to understand the mixing effects at the molecular level and compositional analysis was looked at only briefly. In particular, chemometric methods were not used or discussed. The quantitative analysis of the vibrational spectra is the focus of the present work. Different approaches for evaluation of the spectroscopic data are compared: (1) the calibration of the intensity ratio of characteristic peaks as a function of composition, and (2) chemometrics in terms of principal component analysis (PCA) and inverse least squares regression (ILSR). The intensity ratio approach has the advantage of being very simple and easy to implement, but it may suffer when peaks are overlapping. Chemometric methods are computationally more demanding, but may provide universal applicability.

2 Experimental

2.1 Fuel Blends

A surrogate of gasoline was made by mixing, with a mass ratio of 1:1, iso-octane (2,2,4-Trimethylpentane, Fisher Scientific, >99%) and n-heptane (Fisher Scientific, >95%). Different ratio ethanol-gasoline blends were prepared by increasing the percentage of ethanol (VWR, >99%) in gasoline in steps of 10% by weight. The sample preparation and all measurements were carried out at

atmospheric pressure and a temperature of 294 K. We note that the same samples were studied by IR and excess IR spectroscopy in a previous article[14].

2.2 Raman Spectroscopy

Raman spectra of the blends were recorded using a 90-degree Raman set up, as shown in Figure 1. The samples were in a sealed glass cuvette, in which the light from a HeNe laser (10 mW, 632nm) was focused. The scattered light was collected in a direction perpendicular to the incident laser beam using an achromatic lens. A dielectric long-pass filter (cut-off wavelength 635 nm) blocked elastically scattered laser light. The Raman signal was focused by another achromatic lens onto an optical fiber, which guided the light to an imaging spectrograph (Andor Shamrock, entrance slit 200 micron, focal length 163 mm, grating 1200 lines mm^{-1}). An EM-CCD camera (Andor Newton) eventually detected the dispersed signal. The spectral range from 500 to 4000 cm^{-1} was recorded with a resolution of approximately 6 cm^{-1}.

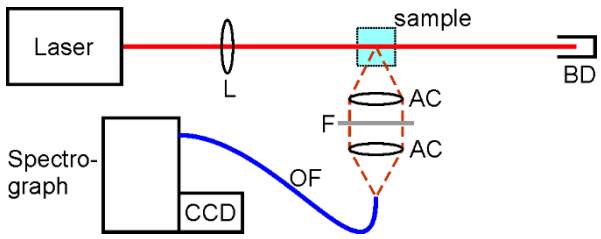

Figure 1: Schematic of the experimental Raman setup. L = lens; BD = beam dump; AC = achromatic lens; F = filter; OF = optical fiber; CCD = charge-coupled device camera.

2.3 IR Spectroscopy

IR spectra of the biofuel blends were collected with a Bruker Vertex v70 spectrometer. The spectral range from 500 to 4000 cm^{-1} was recorded with a

nominal resolution of 1 cm^{-1}. For every sample 32 scans were averaged. The instrument was equipped with an attenuated total reflection (ATR) module (diamond, one reflection, 45°). During the measurements, the samples on the ATR crystal were covered with a small glass cap to avoid sample evaporation.

3 Results and Discussion

In this section the Raman and IR spectra obtained are briefly presented, discussed and compared. Thereafter, two different methods to extract quantitative information from both Raman and IR spectra were used. The ethanol concentration in the mixtures was determined by using (1) the intensity ratio approach and (2) principal components regression (PCR).

3.1 Infrared and Raman spectra

The IR and Raman spectra of the gasoline surrogate, the pure ethanol, and the blends are shown in Figure 2. The different selection rules for IR and Raman are evident in the spectra of the pure substances. In general, a vibrational mode is IR-active when the dipole moment changes during the vibrational motion, and it is Raman-active when the polarizability changes during the vibrational motion.[20, 21] Some peaks are strong in one spectrum and weak in the other, and vice versa. Furthermore, some features appear in the IR spectra, but not in the Raman ones and vice versa.

A detailed analysis and assignment of the individual peaks can be found in previous articles [14, 22] and the references therein, and hence only a brief overview is given here. The characteristic and broad OH stretching band of ethanol can be found in the region between 3000 and 3600 cm^{-1}. The CH

stretching modes of ethanol and the hydrocarbons are located between 2800 and 3100 cm^{-1}. The OH is strong in the IR while the CH dominates the Raman spectrum. The range below 1600 cm-1 is commonly referred to as the fingerprint region. Between 1200 and 1600 cm^{-1}, the CH bending modes can be found. The peak doublet between 1000 and 1100 cm^{-1} can be attributed to the symmetric and asymmetric CO stretches of ethanol with contributions from CH rocking modes. Below 1000 cm^{-1}, the CC stretching modes can be identified as well as a broad OH deformation band from ethanol.

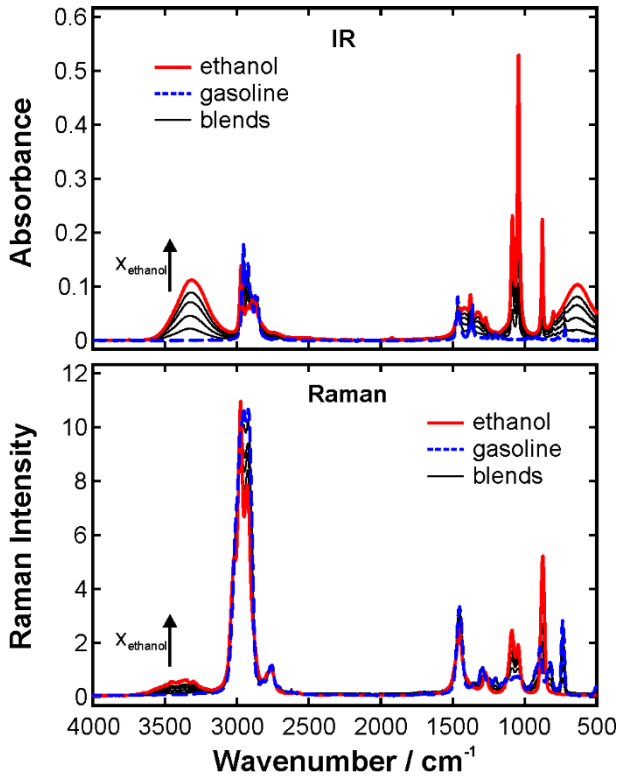

Figure 2: IR and Raman spectra of the pure ethanol (red), pure gasoline (dashed blue), and the blends (black).

The CH stretching region was employed for the quantitative measurements in various ways in this work. Therefore, Figure 3 shows this region of both the IR and the Raman spectra. Both sets of spectra exhibit four isosbestic points in the

CH stretching region. These points represent the wavelengths at which both substances have the same IR absorbance or Raman intensity and their mixtures behave as ideal solution.

The IR peaks from ethanol at 2973, 2928, and 2881 cm^{-1} are usually assigned to the CH_3 antisymmetric stretching, the CH_3 symmetric stretching and the CH_2 symmetric stretching, respectively. However, from a Raman study of a series of alcohols, Atamas et al.[23] suggested that the peaks, which they observed at 2974 and 2873 cm^{-1} can be a result of the Fermi resonance between the fundamental vibration ~2930 cm^{-1} and the overtones of two vibrations at ~1450 and 1470 cm^{-1}. In our case, this means that the peaks at 2973 and 2881 cm^{-1} may be due to Fermi resonances between the fundamental vibration at 2928 cm^{-1} and the CH bending overtones at 1455 and 1479 cm^{-1}. Later, Yu at al.[24] carried out a more detailed analysis by comparing the Raman spectrum of gaseous and liquid ethanol. They concluded that the two spectra present very similar features, except for an enhancement of the CH_3 antisymmetric band and the red shifted band positions in the liquid phase. They assigned the band at ~2881 cm^{-1} to the overlapping symmetric stretching vibrational modes of both CH_2 and CH_3. The band at ~2938 cm^{-1} was assigned to two symmetric -CH_3 Fermi resonances and the weak CH_2 antisymmetric stretching mode. The band at ~2983 cm^{-1} was assigned to the symmetric CH_2 Fermi resonance and the weak CH_3 antisymmetric stretching mode.

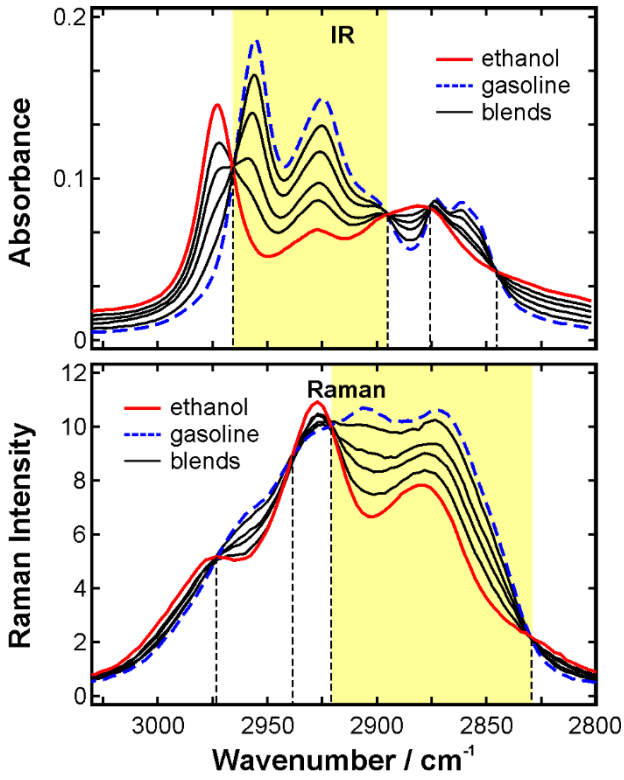

Figure 3: CH stretching region in the IR and Raman spectra of the pure ethanol, pure gasoline, and the blends. The highlighted areas indicate those spectral ranges, which are referred to as 'limited CH range' in the text. The dashed vertical lines indicate the positions of the isosbestic points.

3.2 Intensity ratio approach

The intensity ratio approach is a straightforward method to get quantitative information from a vibrational spectrum. It allows calibrating the intensity ratio of two characteristic peaks from different species against the mixture composition. This method is often used as it is very robust compared to calibrating a single peak as a function of composition [25]. The latter approach would require highly stable radiation sources and detectors as any fluctuation would immediately translate into a significant and systematic measurement error.

The most commonly used bands for the intensity ratio method in mixtures containing alcohols and hydrocarbons are the OH and CH stretching bands. They provide strong signals and are spectrally well separated from the excitation wavelength in a Raman experiment. Hence, they are normally not influenced by interference from elastically scattered light and laser-induced fluorescence. The former can be an issue in field studies when the fluid under investigation contains droplets or particles, which scatter large amounts of photons elastically [26, 27]. The latter may become a problem when the fluid contains aromatic compounds or dyes [28-30], both of which are typical in commercial fuels.

3.2.1 Spectral window selection

The first step towards reproducible and accurate composition measurements using the intensity ratio method is the selection of suitable spectral windows, over which the signal is integrated before the ratio is calculated. This is done in order to maximize the signal to noise ratio and thus to minimize the statistical uncertainty. As a first attempt, the full CH stretching band is utilized and secondly, the window is limited to the region between those isosbestic points, between which the gasoline signal dominates, in order to maximize the sensitivity of the ratio. The regions are indicated in Fig. 3. For the IR spectra, this approach has shown to be beneficial in our previous work [14]. Whether or not it is advantageous in the exploitation of the Raman spectra as well will be examined in the following.

To determine the robustness of the calibration curves, a leave one-out cross validation was carried out. For this purpose, one data point is removed from the calibration data set. The calibration function is then determined from the

235 remaining data points. Eventually, the absorbance (IR) or intensity (Raman)
236 value of the removed data point is fed into the calibration function as a blind
237 value in order to determine the ethanol mass fraction. This procedure was
238 repeated with all individual data points. Plotting the difference between the
239 actual mass fraction (gravimetric value) and the calibrated value for every
240 compositions yields an estimate of the measurement uncertainty and the
241 robustness of the calibration method.
242 Figure 4 compares the Raman and IR calibration curves. The trends of the curves
243 are very similar, but the OH band in the Raman spectra is relatively weak so that
244 the absolute numbers of the OH/CH ratio are a factor of ~20 lower than in IR. In
245 both Raman and IR a narrowing of the spectral window results in an increase in
246 sensitivity. This can be deduced from the steepness of the slopes of the
247 calibration curves. The steeper the slope, the higher the sensitivity.
248 The residuals from the leave-one-out cross-validation, i.e. the deviation of the
249 predicted values from the actual concentration values, are plotted in Figure 5.
250 Generally, a comparable quality of the results can be found for both methods.
251 Larger deviations can be observed at the low and high ethanol concentration
252 ends of the diagrams. This is reasonable, as the calibration functions in these
253 cases have to be extrapolated in order to find a concentration value.
254

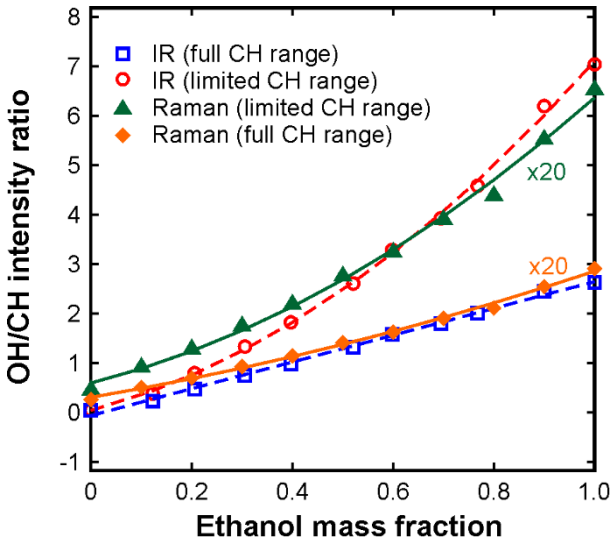

Figure 4: Calibration curves for the intensity ratio of the OH and CH stretching bands in the Raman and IR spectra. The solid and the dashed lines represent best-fit functions of the Raman and IR data, respectively. The Raman data are multiplied by a factor of 20.

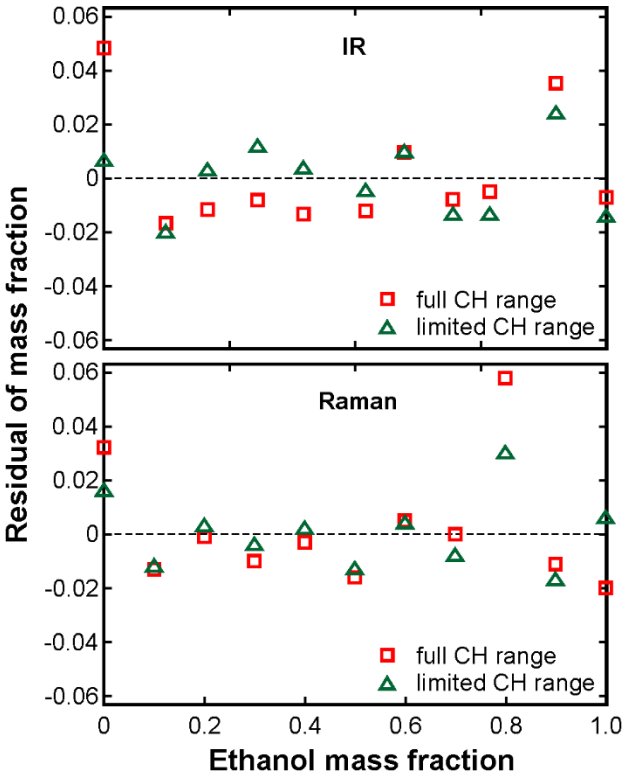

Figure 5: Residuals from the leave-one-out cross validation. Difference between the predicted ethanol concentration, and the actual ethanol concentration in the IR, and Raman spectra.

3.2.2 Influence of Noise

In a practical application, the signal to noise level in the spectra recorded can vary substantially depending on the environment in which the measurement is carried out. In order to test the accuracy of the intensity ratio method, different levels of noise were added to the IR and Raman spectra. Figure 6 shows CH and OH region of the ethanol IR and Raman spectra with 10% of added noise. The noise represents a uniform random distribution with a maximum value corresponding to the value of the maximum peak in the CH stretching region. In the 10% noise case, for example, this means that a uniformly distributed random noise with minimum value zero and maximum value of 10% of the absorbance (IR) or intensity (Raman) value of the strongest peak in the CH stretching region was added to the spectrum.

For each level of noise, the IR and Raman calibration curves, considering the full CH and the limited CH windows, were obtained and a leave-one-out cross-validation was carried out again. The same procedure was repeated 100 times, testing different random noise matrices. The root mean square error (RMSE) normalized with respect to the mean of the predicted ethanol concentration values (coefficient of variation of the RMSE), determined from each calibration from the gravimetrically set values, was calculated. The RMSE is an indicator of the difference between the predicted values and the actual values. The resulting coefficients of variation of the RMSE vs. the noise level are shown in Figure 6. Each curve represents the average of 100 curves for the different random noise matrices. Narrowing the CH window has different effects on the measurement accuracy in IR and Raman when the noise level is considered. In the IR plot, the values for the limited CH range case are higher and, in Raman, the opposite behavior can be observed. It must be noted that without addition of noise, the

values in all four cases considered are reasonable similar. The coefficient of variation of the RMSE increases strongly for the Raman data (the values are factor of about three larger). This can be attributed to the low intensity of the OH band in the Raman spectra. When noise is added, this band becomes easily obscured resulting in a reduced measurement accuracy. The strong OH band in the IR spectra provides a robust basis for accurate concentration determination. The IR based curves in Figure 7 change only moderately with increasing noise.

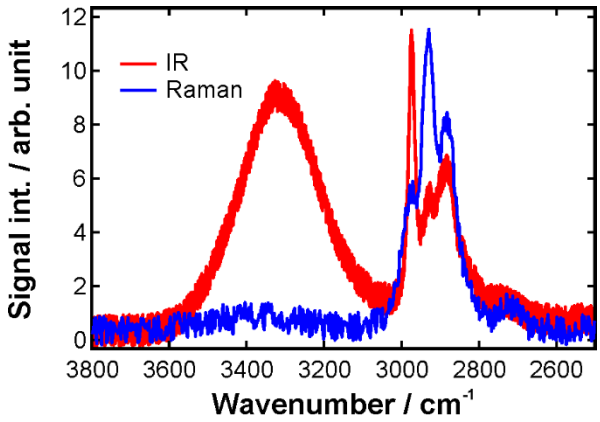

Figure 6: IR and Raman CH and OH regions of ethanol with 10% of noise added.

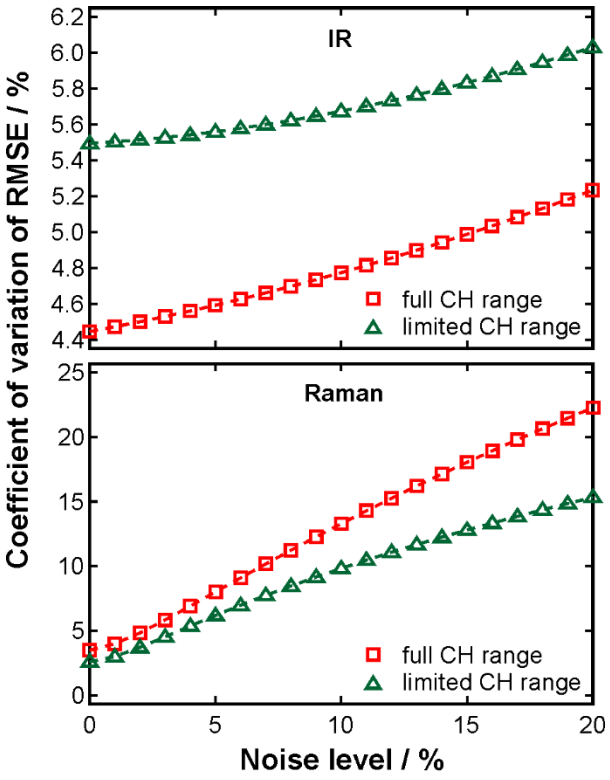

Figure 7: IR and Raman coefficient of variation of the RMSE vs noise level.

3.3 Chemometric approach

Differently from the intensity ratio approach, in which the concentration of the components is calculated from a direct regression of the concentrations onto the intensity/absorbance, the PCR regresses the concentration on the principal components analysis (PCA) scores. Another important difference is that the chemometric method can take the full spectrum into account rather than relying on limited regions.

The PCA has a primary scope to decrease the number of correlated variables representing the set of measured data. This is done by a linear transformation of the variables, which can be visualized as a set of coordinates (one axis per variable), projecting the original ones in a new Cartesian system, in which the variables are sorted in descending order of variance. Therefore, the variable with

316 higher variance is projected onto the first axis, the second on the second axis and
317 so on. The reduction of the number of variables is achieved by considering just
318 those with higher variance between the new variables. Details can be found, e.g.,
319 in the text of Jolliffe[31]. PCA can also be considered as a form of multidimensional
320 scaling. It is a linear transformation of the variables into a lower dimensional
321 space, which retain maximal amount of information about the variables. The new
322 variables, differently from the original ones, are uncorrelated and are called
323 principal components. The PCA scores represent a summary of the relationship
324 among the observations, the loading a summary of the variables. A regression
325 method can then be used to correlate the principal components with the quantity
326 to be measured. In our case, PCR combines PCA and an Inverse Least Squares
327 regression (ILSR) to solve the calibration equation for the spectra [32, 33]. More
328 sophisticated approaches such as support vector machines (SVM)[34] and artificial
329 neuronal networks (ANN)[35] are not necessary for the relatively simple system to
330 be analyzed here, but they may be an option when real multicomponent fuels are
331 the subject of investigation.
332
333 **3.3.1 Spectral window selection**
334 As mentioned above, the chemometric method can in principle be applied to the
335 full spectrum. For better comparability, we performed additional PCR analyses
336 using the same spectral regions as for the intensity ratio method: the full CH
337 stretching region and the limited CH stretching region. The residuals from the
338 PCR, i.e. the deviation of the predicted mass fraction from the actual mass
339 fraction, were calculated and they are shown in Figure 8. The values of the
340 residuals are slightly smaller than the ones obtained by predicting the ethanol

mass fraction using the intensity ratio approach. This is reasonable as more spectral information is taken into account.

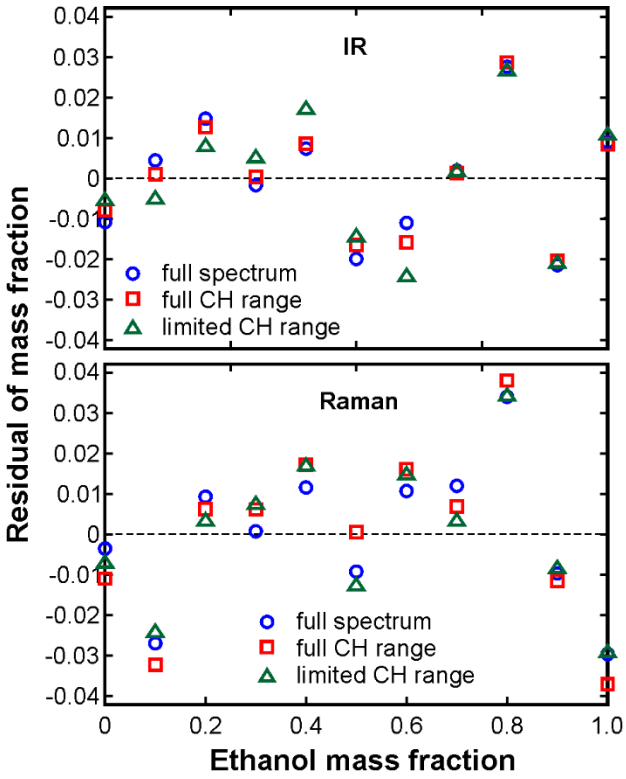

Figure 8: Residuals from the PCR. Difference between the predicted ethanol mass fraction, and the actual ethanol mass fraction determined from the IR and Raman spectra.

To validate the model, again a leave-one-out cross-validation was carried out. For this purpose, a vector of the intensity of a single ratio blend is taken out from the matrix of all the blends. A PCA is performed on the new matrix. Eventually, the ethanol mass fraction value of the blend corresponding to the removed vector is fed into the PCR curve as a blind value in order to determine the composition. This procedure was repeated with all individual vectors. The residuals of the cross-validation, i.e. the differences between the actual responses and the cross-validated fitted values, are shown in Figure 9. The residuals measure the predictive ability of the model. Selecting different portions

of the spectrum, the resulting residuals are similar. The values are comparable with the ones obtained by using the intensity-ratio method.

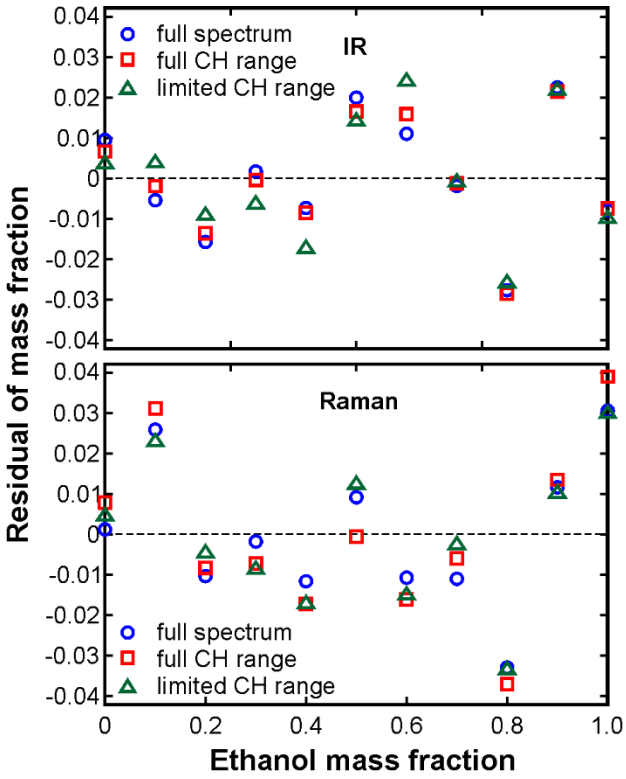

Figure 9: Residuals from the leave-one-out cross validation for the IR and Raman data.

3.3.2 Influence of Noise

To test the accuracy of the method, different levels of noise have been added to the Raman and IR spectra, as previously done for the intensity ratio method. A PCR analysis of each spectrum, considering the full spectrum, the full CH stretching band, and the limited CH stretching band, with different noise levels was done. A leave-one-out cross-validation was carried out for each PCR curve to determine the predicted ethanol concentration. As previously done with the intensity ratio approach, 100 different random noise matrices were used. The root mean square error (RMSE) normalized with respect to the mean of the predicted values (coefficient of variation of the RMSE) and the coefficient of

373 determination R^2 vs. the noise level are shown in Figure 10. The R^2 values
374 indicate the goodness of the linear fit of the predicted concentration vs. the
375 actual concentration curve. The closer R^2 is to 1 the better is the correlation
376 between the data points. Each curve in the plots represents the average of 100
377 curves (each one done by using a different random noise matrix).
378 The change in the coefficient of variation of RMSE with the noise level suggests
379 that the PCR is more accurate if the entire spectrum is considered. In contrast to
380 the intensity ratio method, narrowing the window selection leads to a loss in the
381 accuracy in predicting the mass fraction. When the full spectrum is considered,
382 there are more spectral data points making the model less susceptible to spectral
383 noise. The R^2 values confirm for both Raman and IR a better correlation between
384 the predicted concentration and the actual one if a larger portion of the spectrum
385 is used. One reason is that the strong features associated with the symmetric and
386 asymmetric CO stretches of ethanol at 1046 and 1088 cm^{-1} contribute. Regarding
387 the results obtained from the full IR spectra it can be concluded that the noise
388 level has almost no influence on the accuracy. In other words, the method is very
389 robust. The corresponding Raman data show a moderate decrease in accuracy
390 when the level of noise exceeds ~5%. The R^2 value deceases monotonically from
391 ~0.997 at 5% to ~0.986 at 20%, which is acceptable in many applications.
392 The comparison of the chemometric results with the ones obtained with the
393 intensity ratio method reveals an improvement when the PCR is used for both IR
394 and Raman. This is particularly true when the full spectral range is exploited in
395 the analysis. However, it should be noted that the improvement is more
396 significant on the Raman side as the weak OH band of ethanol is no longer the
397 only characteristic feature taken into account.

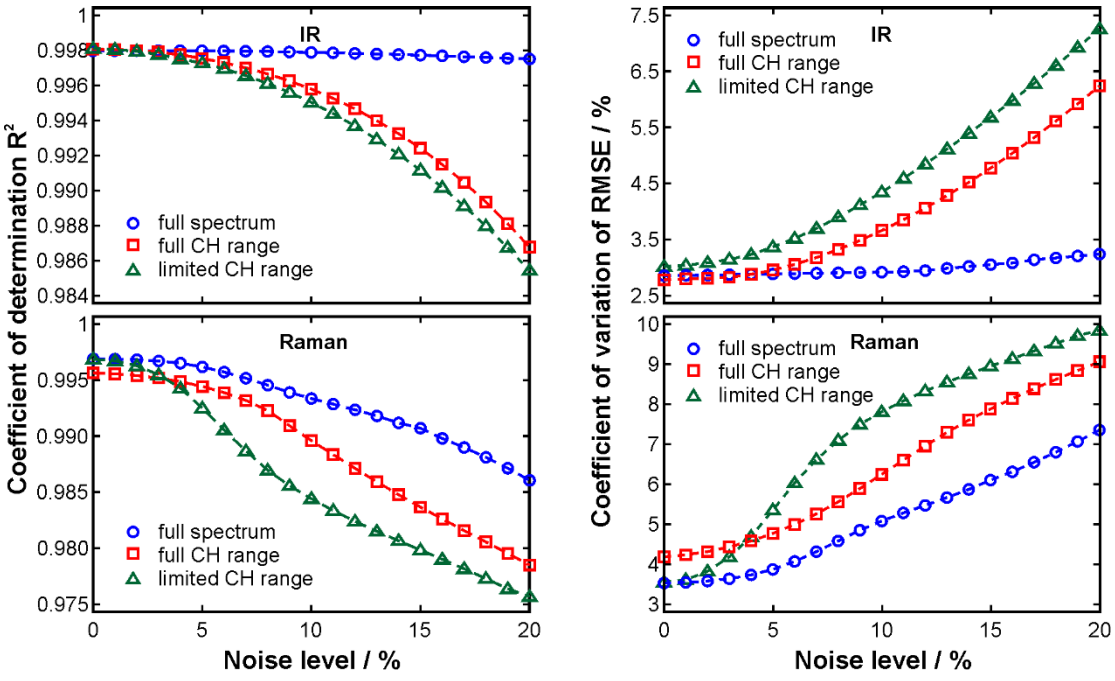

Figure 10: Coefficient of determination R^2 and coefficient of variation of the RMSE vs. noise level calculated for both Raman and IR data.

4 Summary and Conclusion

In this paper we have used Raman and IR spectroscopy to determine the ethanol content in ethanol/gasoline blends. For this purpose, two different evaluation methods to extract quantitative information from the spectra have been compared. The first method was the commonly used approach of an intensity ratio calibration. Secondly, Principal Components Regression (PCR) has been used.

Using the intensity ratio method, an enhancement of the sensitivity and accuracy in predicting the blend composition has been achieved by narrowing the spectral window in the CH stretching region for both Raman and IR. On the contrary,

using the PCR led to a better accuracy when the full spectrum was considered. Overall, the uncertainty of the two methods has been found comparable. The PCR method seemed to be more accurate in predicting the blend composition than the intensity ratio method when applied to the Raman spectra, but not when applied to the IR ones. However, a higher accuracy can be obtained at the expense of a loss of simplicity of the approach.

In order to find the method of choice for a given application, a number of further points must be taken into account. IR spectroscopy has advantages in the analysis of opaque samples, as ATR probes can record spectra in non-transparent samples. It may also be more suitable when the samples contain a high amount of fluorescing species. A problem, on the other hand, may be high amounts of water as the water absorption is very strong, virtually across the entire mid-infrared spectral range. Also, the costs and dimensions for a high-quality IR instrument may be an issue. Raman spectroscopy is well suited when the samples are transparent in the spectral region under study. The arbitrary choice of the excitation wavelength provides some flexibility here. This is also an advantage when the use of fiber probes is necessary. Employing visible lasers for excitation allows the use of very long optical fibers, while the length of ATR probes in IR spectroscopy is normally limited to a few meters due to the poor transmission. Moreover, Raman instruments with dispersive elements can be made very compact and are ideally suited for field measurements. With the costs for sufficiently sensitive miniature spectrometers decreasing, the implementation of Raman spectroscopy as versatile and portable sensors seems very promising.

Acknowledgements

This work was supported by the Northern Research Partnership (NRP) in Scotland. The authors thank Florian Zehentbauer for technical assistance during the Raman experiments.

References

1. Y. Lin and S. Tanaka, *Applied Microbiology and Biotechnology*, 2006, **69**, 627-642.
2. M. Balat and H. Balat, *Applied Energy*, 2009, **86**, 2273-2282.
3. T. Wiesenthal, G. Leduc, P. Christidis, B. Schade, L. Pelkmans, L. Govaerts and P. Georgopoulos, *Renewable and Sustainable Energy Reviews*, 2009, **13**, 789-800.
4. M. Koc, Y. Sekmen, T. Topgül and H. S. Yücesu, *Renewable Energy*, 2009, **34**, 2101-2106.
5. S. Lehmann, S. Lorenz, E. Rivard and D. Brüggemann, *Exp. Fluids*, 2015, **56**, 1871.
6. H. Bayraktar, *Renewable Energy*, 2005, **30**, 1733-1747.
7. L. C. Lichty and C. W. Phelps, *Industrial and Engineering Chemistry*, 1938, **30**, 222-230.
8. D. Turner, H. Xu, R. F. Cracknell, V. Natarajan and X. Chen, *Fuel*, 2011, **90**, 1999-2006.
9. R. P. Philp, *HRC-Journal of High Resolution Chromatography*, 1994, **17**, 398-406.
10. R. A. Cross, *Nature*, 1966, **211**, 409.
11. N. Segudovic, T. Tomic, L. Skrobonja and L. Kontic, *Journal of Separation Science*, 2004, **27**, 65-70.
12. J. Kiefer, *Energies*, 2015, **8**, 3165-3197.
13. H. C. Van Ness, J. Van Winkle, H. H. Richtol and H. B. Hollinger, *J. Phys. Chem.*, 1967, **71**, 1483-1494.
14. S. Corsetti, F. M. Zehentbauer, D. McGloin and J. Kiefer, *Fuel*, 2015, **141**, 136-142.
15. Q. Ye, Q. Xu, Y. Yu, R. Qu and Z. Fang, *Opt. Commun.*, 2009, **282**, 3785-3788.
16. D. R. Battiste, S. E. Fry, F. T. White, M. W. Scoggins and T. B. McWilliams, *Anal. Chem.*, 1981, **53**, 1096-1099.
17. R. M. Balabin, R. Z. Syunyaev and S. A. Karpov, *Energy and Fuels*, 2007, **21**, 2460-2465.
18. P. Ravi Prasad, K. S. Rama Rao, K. Bhuvaneswari, N. Praveena and Y. V. V. Srikanth, *Energy Sources A*, 2008, **30**, 1534-1539.
19. M. K. Ahmed and J. Levenson, *Petroleum Science and Technology*, 2012, **30**, 115-121.

20. H. Haken and H. C. Wolf, *Molecular Physics and Elements of Quantum Chemistry* Springer, Heidelberg, 1995.
21. C. N. Banwell and E. M. McCash, *Fundamentals of Molecular Spectroscopy*, McGraw Hill, London, 4th edn., 1994.
22. K. Noack, J. Kiefer and A. Leipertz, *ChemPhysChem*, 2010, **11**, 630-637.
23. N. A. Atamas, A. M. Yaremko, L. A. Bulavin, V. E. Pogorelov, S. Berski, Z. Latajka, H. Ratajczak and A. Abkowicz-Bieńkoc, *J. Mol. Struct.*, 2002, **605**, 187-198.
24. Y. Q. Yu, K. Lin, X. G. Zhou, H. Wang, S. L. Liu and X. X. Ma, *J. Phys. Chem. C*, 2007, **111**, 8971-8978.
25. J. Kiefer, T. Seeger, S. Steuer, S. Schorsch, M. C. Weikl and A. Leipertz, *Meas. Sci. Technol.*, 2008, **19**, 085408.
26. A. Malarski, B. Schürer, I. Schmitz, L. Zigan, A. Flügel and A. Leipertz, *Appl. Opt.*, 2009, **48**, 1853-1860.
27. J. Kiefer, F. Toni and K.-E. Wirth, *J. Raman Spectrosc.*, 2015, **in print**, DOI 10.1002/jrs.4743.
28. D. Patra and A. K. Mishra, *Polycyclic Aromatic Compounds*, 2001, **18**, 381-396.
29. S. D. Harvey and B. W. Wright, *Talanta*, 2011, **86**, 148-156.
30. D. Wei, S. Chen and Q. Liu, *Appl. Spectr. Rev.*, 2015, **in print**, DOI: 10.1080/05704928.05702014.05999936.
31. I. Jolliffe, *Principal component analysis*, John Wiley & Sons, 2002.
32. S. Wold, K. Esbensen and P. Geladi, *Chemometrics and Intelligent Laboratory Systems*, 1987, **2**, 37-52.
33. D. M. Haaland and E. V. Thomas, *Anal. Chem.*, 1988, **60**, 1193-1202.
34. K. Noack, B. Eskofier, J. Kiefer, C. Dilk, G. Bilow, M. Schirmer, R. Buchholz and A. Leipertz, *Analyst*, 2013, **138**, 5639–5646.
35. V. O. Santos Jr., F. C. C. Oliveira, D. G. Lima, A. C. Petry, E. Carcia, P. A. Z. Suarez and J. C. Rubim, *Anal. Chim. Acta*, 2005, **547**, 188-196.